Ocean Sci. Discuss., 12, 2743–2782, 2015
www.ocean-sci-discuss.net/12/2743/2015/
doi:10.5194/osd-12-2743-2015

Ocean Science
Discussions
Open Access

Mesoscale eddies and submesoscale structures of Persian Gulf Water off the Omani coast in Spring 2011

P. L'Hégaret[1], X. Carton[1], S. Louazel[2], and G. Boutin[1]

[1]Laboratoire de Physique des Oceans/UMR6523, UBO, 6 avenue Le Gorgeu CS93837, 29238 Brest CEDEX 3, France
[2]Service Hydrographique et Oceanographique de la Marine, 13 rue de Chatellier CS92803, 29228 Brest CEDEX 2, France

Received: 8 October 2015 – Accepted: 22 October 2015 – Published: 13 November 2015

Correspondence to: P. L'Hégaret (pierre.lhegaret@outlook.com)

Published by Copernicus Publications on behalf of the European Geosciences Union.

Abstract

The Persian Gulf produces a high salinity water (Persian Gulf Water, PGW hereafter) flowing into the Sea of Oman, in the northwestern Indian Ocean. Past the Strait of Hormuz, the PGW cascades down the continental slope and spreads in the Sea of Oman under the influence of the energetic mesoscale eddies with different thermohaline signatures and pathways depending of the season. In spring 2011, the Phys-Indien experiment was carried out in the Arabian Sea an in the Sea of Oman. This study uses the results from the measurements to characterize the water masses, their thermohaline and dynamical signatures. During the spring intermonsoon, an anticyclonic eddy is often observed at the mouth of the Sea of Oman. This structure was present in 2011 and created a front between the eastern and western part of the basin. As well two energetic gyres were present along the Omani coast in the Arabian Sea. At their peripheries, injections of fresh and cold water are found in relation with the stirring of the eddies. The PGW observed below or between these eddies have a different dilution depending of the position and formation periods of the gyres. Furthermore, in the western Sea of Oman, the PGW is fragmented in filaments and submesoscale eddies. As well, recirculation of the PGW is observed, thus having the presence of salty nearby patches with two densities. Offshore, in the Arabian Sea, a submesoscale lens was recorded. The different mechanisms leading to its formation and presence are assessed here.

1 Introduction

The Indian Ocean, the third tropical basin in size, is bounded north by the Asian landmass. The orography of this landmass leads to the existence of monsoons, which strongly influence the regional oceanic circulation. The northwestern part of the Indian Ocean is comprised of different sub-basins, each with specific geographic and climatic characteristics. This study focuses on two of them, the Sea of Oman and the Arabian Sea (see Fig. 1). The Sea of Oman (or Gulf of Oman) connects the Persian

OSD
12, 2743–2782, 2015

Gulf to the Arabian Sea; it deepens along its zonal axis, to 3400 m depth in its eastern part; it also widens from the Strait of Hormuz to its mouth, at Ra’s Al Hadd. The north-western Arabian Sea has a floor below 3500 m depth and is crossed from north-east to south-west by the Owen Fracture Zone, with diving and rising of the topography along the fault. Along the Omani coast a plateau of 200 m depth extends from Ra’s Al Hadd to Ra’s Madrakah (see again Fig. 1 for locations).

The surface circulation around the Arabian Peninsula is dominated by mesoscale eddies formed via different processes, depending on the location and on the time of the year (see Fischer et al., 2002). Al Saafani et al. (2007) identified that such eddies in the Gulf of Aden, which have a westward propagation, are generated by Rossby waves emitted from the Indian coast or in the interior of the basin. This Rossby wave mechanism is also present in the northern Arabian Sea, these waves being forced by wind and by coastal Kelvin waves (see L’Hégaret et al., 2015).

Another formation process of mesoscale eddies is the instability of alongshore currents, during the monsoon seasons (see again L’Hégaret et al., 2015). In summer (winter), these currents are intense and have a negative (positive) altimetric signature as coastal “belts”, which grow under the influence of the wind stress curl. These coastal currents then form meanders and eddies, which have a radius comparable with, or slightly larger than the first baroclinic radius of deformation (about 40 km in the region, see Chelton et al., 1998). These eddies have a strong velocity, above 60 $\mathrm{cm\,s^{-1}}$, near the surface, and a vertical influence on the water masses at depth (see Bower and Furey, 2012; Carton et al., 2012).

Over the Persian Gulf, intense evaporation (see Privett, 1959; Meshal and Hassan, 1986), steady winds and little fresh water inflow (through precipitation and river, see Reynolds, 1993), lead to the formation of highly saline water in the northwestern and southwestern parts of this semi-enclosed sea. This saline water then flows into the Sea of Oman via the Strait of Hormuz. In the Sea of Oman, this dense outflow of Persian Gulf Water (hereafter PGW), equilibrates around 250 m depth, mixing with surrounding

OSD
12, 2743–2782, 2015

and fresher Indian Ocean Surface Water. Near the Strait, PGW has high thermohaline characteristics, with salinity above 39 psu and temperature above 22 °C.

In the Sea of Oman, the upper 100 m of the water column are occupied by the Arabian Sea High Salinity Water, a water mass formed in the northeastern Arabian Sea in winter (see Kumar and Prasad, 1999), which spreads in the western basin through the year. Its thermohaline characteristics in the Sea of Oman and northwestern Arabian Sea are salinity around 36.6 psu and temperature above 22 °C.

In the past, few dedicated cruises provided observations to describe the PGW pathway out of the Persian Gulf and its variations in the Sea of Oman. This PGW outflow is usually presented as a southeastward flow, along the coast of Oman (see Premchand et al., 1986). In October–November (fall intermonsoon), the GOGP99 experiment sampled the Persian Gulf outflow and identified it as a coastal layer, extending to the south of the Sea of Oman (see Pous et al., 2004).

More recently, ARGO floats (see Carton et al., 2012; L'Hégaret et al., 2013) and HYCOM numerical simulations (see L'Hégaret et al., 2015) reveal different offshore ejection mechanisms of PGW under the influence of the mesoscale eddies, in the Sea of Oman. This occurs particularly in spring when a dipole advects this water mass between the Strait of Hormuz and Ra's al Hamra and along the coast of Iran.

In spring 2011, the Phys-Indien experiment was carried out around the Arabian Peninsula, recording the thermohaline and dynamical characteristics of the upper ocean. Submesoscale fragments (and in particular a lens) of Persian Gulf Water were sampled in the Sea of Oman and off Ra's Al Hadd, in the Arabian Sea.

This paper main objective is twofold. First, to describe the mesoscale structures in spring 2011 and their induced circulation on the water masses. Second, to concentrate on the submesoscale fragments detached from or by the mesoscale eddies, and then, on the nature, structure, recurrence and possible role of such fragments.

OSD
12, 2743–2782, 2015

2 Data and method

2.1 Climatologies and long time observations

Altimetric maps are obtained from the AVISO satellite data center; these maps are created via data merger from Jason 1, Jason 2 and Envisat measurements (see Ducet et al., 2000; Rio et al., 2011). The along-track data are then interpolated on a $1/4^\circ \times 1/4^\circ$ Mercator grid with a daily value. The error on along-track measurements of sea level are 3–4 cm (see Fu and Cazenave, 2000). Adding a 22 year mean of the sea surface topography, mean absolute dynamic topography (MADT) is generated. In each MADT map, an spatial (and instantaneous) average is subtracted, to obtain anomalies of the sea surface elevation (MADT anomalies).

The wind stress and wind stress curl are obtained from the ASCAT database of Ifremer, with a daily mean and a $1/4^\circ \times 1/4^\circ$ horizontal resolution, from 2007 to 2014.

To acccurately describe the water masses, the Generalized Digital Environment Model (GDEM) climatology is used (http://www.usgodae.org/). It provides monthly mean salinity and temperature maps, with 72 vertical levels and a $1/4^\circ \times 1/4^\circ$ horizontal resolution (see Teague et al., 1990). These maps are modified by merging measurements from ARGO floats (from the ANDRO database see Ollitrault and Rannou, 2013). About 300 floats, with periods varying between 5 and 10 days, sampled the Arabian Sea and between 2002 and 2014. This provides enough profiles for monthly corrections of the climatology in each sub-basin. This correction is calculated as follows: first, each float measurement is converted into an anomaly by substracting the climatological value at the given time and location. Second, this pointwise anomaly was extended spatially with an isotropic Gaussian correlation function, weighted by the local number of data (the radius of the Gaussian was chosen as $L = 50$ km, typical of a mesoscale eddy). This correlation function was normalized to unity, where data lay. Third, the resulting anomaly is added to the climatology (see Fig. 2, left and center). The third panel of this figure (right) indicates the number of profiles, with their radii of correlation.

OSD
12, 2743–2782, 2015

2.2 The Phys-Indien 2011 measurements

The Phys-Indien 2011 experiment measured the circulation and water masses in the sub-basins around the Arabian Peninsula, from the Red Sea to the Persian Gulf from late February to April 2011, using many devices (CTD on Seasoar, CTD and L-ADCP stations, XBT, XCTD casts, en-route VM-ADCP, release of Surdrift buoys and of Provor floats, collection of meteorological data; see the sections on Fig. 3). This study focuses on the measurements in the northwestern Arabian Sea and in the Sea of Oman, in March 2011, with a high-resolution snapshot of the thermohaline and dynamical characteristics of the region obtained by the experiment. In particular, these sections crossed mesoscale eddies and the PGW outflow and fragments.

The thermohaline sections were obtained with two CTD's on a SeaSoar, a towed device. Pressure, temperature and conductivity are thus obtained in the upper 350 m of the water column with accuracies of 10^{-3} °C, 3×10^{-4} S m^{-1} and 0.015 % of the pressure value). Salinity is calculated from temperature and conductivity. In this region, strong horizontal and vertical thermohaline gradients occur, which lead to biases in temperature and salinity data on seasoars. These biases are due to thermal inertia of the sensors, most occur between the lowering and rising of the device, which result in a delay between the conductivity and temperature measurements (see Barth et al., 1996). These errors can be corrected by applying a couple of coefficients, a first one correcting the amplitude of the measurements between the rising and lowering of the SeaSoar, and a second coefficient correcting the time delay (see Lueck and Picklo, 1990). Once corrected, the SeaSoar measurements are validated using independent CTD station or XCTD casts data (such stations or casts are achieved along the SeaSoar transects). The relative residual error of the corrected SeaSoar salinity remains below 0.5 % of the CTD's.

The horizontal velocity was obtained with a 38 kHz Vessel Mounted – ADCP (VM-ADCP hereafter); this device provides data most often from the surface to about 1000 m depth, with an accuracy of 5×10^{-3} m s^{-1} (in a few instances, deeper reach, down to

1600 m, is obtained for the VM-ADCP). This device produces high resolution measurements but is sensitive to noises due to small scale dynamical processes or to biological activity. A low pass filter is applied to the signal keeping the structures with a size superior to 3 km, to focus on the submesoscale and mesoscale processes. Another VM-ADCP, with 150 kHz frequency, was activated but its data are not shown here (due to too shallow reach). These data are used nevertheless to validate the 38 kHz ADCP measurements in the upper ocean. The VM-ADCP data are filtered, but a few sections were interrupted or were too noisy, thus having blanks. No interpolation is then carried out and the blanks are displayed on the figures. This may also be the case of a few SeaSoar transects.

During Phys-Indien, five drogued Surdrift buoys were deployed and programmed for 180 days of recording. These surface buoys are connected to a large holey-sock drogue by a thin Kevlar cable, 80 to 250 m long. A test on the acceleration of each buoy was applied to determine a possible loss of the drogue. These buoys were positioned by Argos, their trajectories were sampled every hour and a thermistor sensor gave the surface temperature at each recording.

Also, 6 PROVOR floats were deployed during this cruise. They were positioned via Argos when they surfaced at the end of each 5 day cycle. These floats were equipped with a CTD probe providing temperature, conductivity and pressure with an accuracy of 0.01 °C, 10^{-3} S m^{-1} and 1 dbar respectively. Their parking depth was programmed to 700 dbar instead of 1000 dbar; they dived to 2000 dbar every 5 days and acquired data while rising to the surface, where these data were transmitted.

2.3 Thermodynamical and dynamical quantities derived from the measurements

To describe the structure of the mesoscale eddies, surface maps of MADT anomaly are computed at the period and location of Phys-Indien measurements; from this anomaly, surface geostrophic velocities (U, V), relative vorticity and the Okubo Weiss quantity are obtained through derivations. The Okubo–Weiss quantity is defined as a difference, (in norm) between deformation and relative vorticity

$$\mathrm{OW} = \sigma_{\mathrm{strain}}^2 + \sigma_{\mathrm{shear}}^2 - \omega^2$$

with the shear,

$$\sigma_{\mathrm{shear}} = \frac{\partial V}{\partial x} + \frac{\partial U}{\partial y}$$

the strain

$$\sigma_{\mathrm{strain}} = \frac{\partial U}{\partial x} - \frac{\partial V}{\partial y}$$

and the relative vorticity

$$\omega = \frac{\partial V}{\partial x} - \frac{\partial U}{\partial y}.$$

The Okubo–Weiss quantity is positive in regions where deformation dominates rotation, and it is negative where vorticity dominates. It is calculated in the upper 350 m of the water column using density from the ARGO-GDEM climatology.

From the thermohaline data, density and spiciness are calculated along the sections. In situ density is obtained by a state equation from IOC and IAPSO (2010). Density anomaly σ_0 is displayed. Using T_0, S_0 and ρ_0, the reference temperature, salinity and density, of 20 °C, 37 psu and 998 kg m^{-3}, spiciness γ is calculated:

$$\gamma = \gamma_0 \left[1 + \alpha (T - T_0) + \beta (S - S_0)\right].$$

Using these SeaSoar density fields and surface velocity calculated from MADT from AVISO, sections of geostrophic velocities are computed in order to compare them with the VM-ADCP velocity measurements.

OSD
12, 2743–2782, 2015

Using velocities from the VM-ADCP measurements and density from the SeaSoar it is possible to calculate a two-dimensional Ertel potential vorticity (EPV) (see Hoskins, 1974).

$$\mathrm{EPV} = f\left(f + \frac{\partial V_g}{\partial x}\right)\frac{\partial b}{\partial z} - f\frac{\partial V_g}{\partial z}\frac{\partial b}{\partial x}$$

with $b = -(\frac{g}{\rho_0})\rho$ the buoyancy.

Note that these calculations lead to some noise in the results; the figures presented in the text are slightly filtered for legibility.

3 Mesoscale situation from late 2010 to mid 2011

The spring inter monsoon extends on average from February to May in the Arabian Sea. During this period the wind stress over the basin is low, between the two local maxima of the winter and summer monsoon. The wind stress curl is positive in winter and negative in summer with strongest values. Intermonsoon periods show a change in sign of the curl and weak winds.

The wind stress from summer 2010 to summer 2011 (see Fig. 4), followed the climatological tendency with two peaks, one in summer and a second one in winter, with the lowest values observed in late September 2010 and from February to mid April 2011. The variations of the wind stress curl displayed the winter plateau from November 2010 to the end of January 2011 and the strongest values starting from late May. Both graphs indicate a spring inter monsoon taking place from February to May 2011. Furthermore, the winds stress curl off Ra's Al Hadd (see Fig. 4, right) changed sign during this period, being positive from mid February to mid March, and then negative until May. A positive slope in the wind work, linked to a negative slope of wind stress curl, then deepens the vorticity distribution for surface eddies (see L'Hégaret et al., 2015; Vic et al., 2014).

OSD
12, 2743–2782, 2015

On Fig. 5, the MADT anomaly is displayed over the Sea of Oman and the northwestern Arabian Sea from the winter monsoon to the beginning of the summer monsoon (November 2010 to June 2011).

In November 2010, an alongshore current, associated with a positive MADT anomaly, flowed along the southern coast of Oman (L'Hégaret et al., 2015); it was driven by the Ekman currents. This current started to meander, and the wavelengths were about $2\pi R_d$ where R_d is the first baroclinic radius of deformation (40 km). Offshore of this coastal current, mesoscale cyclones (C1) exitted the Sea of Oman and propagated southwestward along the coast of Oman. Their surface temperature is colder than that of the surrounding waters. The Owen fracture zone and the coastal current can jointly channel these cyclones along the coast (C1 and C2).

From December 2010 through February 2011, the MADT anomaly was positive in the Sea of Oman, with the onset of a large anticyclonic eddy (A1), and higher surface temperature whereas colder waters exitted through the Strait of Hormuz. This anticyclone was part of a dipole, located nearly every year in spring near Ra's al Hamra (see L'Hégaret et al., 2013). South of Ra's Al Hadd, in the Arabian Sea, the alongshore current formed an anticyclone (A2), which splitted apart the C1 and C2 cyclones at Ra's al Hadd. The first cyclone (C1) remained east of Ra's Al Hadd until April; the second part of the cyclone (C2) drifted southwestward, slowly warming up and decreasing in intensity.

From March through May 2011, A1 splitted in two anticylones, A1 and A3. Three main vortices line up along 61° E, south and north of Ra's Al Hadd: the anticyclone at the mouth of the Sea of Oman (A3), the cyclone at Ra's al Hadd (C1) and the anticyclone south of it (A2).

In May–June 2011, the sea surface warmed up, cyclone C1 weakens, A2 intensifies in relation with the increasing negative wind stress curl and the alongshore current formed again in response to the onset of the summer monsoon.

The observed evolution of the structures in the region during the spring 2011 follows that of an average spring inter monsoon, with large structures dominating the surface

OSD
12, 2743–2782, 2015

circulation and a strong anticylonic signature in the eastern Sea of Oman. The eddies influence the distribution of the sea surface temperature, intensifying the thermal front near Ra's al Hadd (and later on advecting cold water offshore); they also have an influence at depth, in particular the anticyclone in the eastern Sea of Oman can eject the PGW offcoast towards the northern Iranian coast, and advects these waters around it (already mentioned in Carton et al., 2012). This will be evidenced now with the Physindien experiment data.

4 Vertical structure of mesoscale eddies in the region in Spring 2011, and relation to PGW

This section focus on the vertical characteristics of the eddies presented earlier and their relations to the PGW, through the Physindien experiment results. Figure 6, presents the surface fields of interest during the period of measurements, from the 16 to 30 March 2011; from the MADT, the relative vorticity, Okubo–Weiss parameter and geostrophic velocities are calculated through derivations. The positions of three sections of interest are indicated on these maps. A first one focuses on the Arabian Sea (AS section), a second one on the Sea of Oman (SO section) and a last one crosses a submesoscale off Ra's Al Hadd (lens section). These sections present velocities measured with the VM-ADCP and geostrophic velocities, density and spice, Okubo–Weiss and Ertel Potential Vorticity fields (see Sect. 2 for computation).

4.1 Arabian Sea

The Arabian Sea (AS) section studied here is located in the Arabian Sea, south of Ra's Al Hadd, from 16 to 22° N almost along 60° E; it was carried out from 16 to 19 March 2011. The MADT anomaly map (Fig. 6, top, left) and the relative vorticity map (Fig. 6, top, left) indicate that section AS intersected, from south to north, a cyclone (C2), and a stronger anticyclone–cyclone pair (A2–C1). Cyclone C2 is part of a three cyclone compound, south of A2–C1. These cyclones were intensified in January 2011 by a westward propagating, negative MADT anomaly, generated earlier from the east.

The map of surface relative vorticity confirms that C2 was weak ($\varpi < 10^{-5}\,s^{-1}$). Cyclone C1 was the strongest eddy ($\varpi > 3 \times 10^{-5}\,s^{-1}$) and the anticyclone A2 had $\varpi \sim -1.5 \times 10^{-5}\,s^{-1}$ (Fig. 6, top, right). The fastest velocities ($60\,cm\,s^{-1}$) were located on a ring around cyclone C1 and on the jet between A2 and C1 (Fig. 6, bottom, right). A2 also presented strong surface velocities, above $35\,cm\,s^{-1}$.

The Okubo–Weiss field (Fig. 6, bottom, left) indicates maximal deformation around cyclone C1 and on the A2–C1 jet.

The velocity structure of the eddy has a strong geostrophic component (see Fig. 7, top). The measurements indicated stronger values in the eddies, between 100 and 150 m depth with maximum velocity, above $80\,cm\,s^{-1}$, than those computed geostrophically. The front between the cyclone and anticyclone is observed at the same position in both velocity sections. Furthermore this velocity remained noticeable below 600 m depth, with values above $10\,cm\,s^{-1}$ (not shown). This confirms the deep dynamical influence of these eddies and their barotropic component.

The EPV and Okubo–Weiss help identify the coherent structures (see Fig. 7, center). The maximal values are found in the core of the eddies, positive for the cyclones C1 and C2 and negative for the anticyclone A2, between 50 and 150 m depth. Furthermore, the position of these maxima are correlated with a negative Okubo–Weiss quantity, meaning that rotation dominates deformation, whereas the periphery of the eddies are characterized by predominance of deformation over rotation.

The thermohaline sections (Fig. 7, bottom) show three water masses. The upper layer, down to about 100 m depth, contains Arabian High Salinity Water (ASHSW), with temperature between 22 and 26 °C, salinity above 36.5 psu and potential density below $25\,kg\,m^{-3}$. ASHSW is the saltiest and spiciest water recorded along this section. Persian Gulf Water (PGW) is found between about 200 and 350 m with temperature ranging from 17 to 20 °C and salinity varying between 36.2 and 36.4 psu, with a potential density between 25.9 and $27\,kg\,m^{-3}$ (see Thoppil and Hogan, 2009). The third water mass is the Indian Ocean Central Water (IOCW), observed between the two salty water masses and below the PGW; with temperature between 14 and 18 °C and salinity between 35.6 and 36.1 psu.

The depths and characteristics of these three water masses are strongly influenced by the mesoscale eddies, as revealed on the density and spiciness sections (Fig. 7, bottom). The anticyclone and the cyclone induced a vertical stretching or squeezing of the isopycnals. The depth of ASHSW varied thus from 150 m depth, below the anticyclone, to 80 m depth below the cyclone. Similarly, PGW lied between 250 and 350 m depth under anticyclone A2, 50 m deeper than out of the eddies. PGW shoaled under cyclone C1, between 180 and 300 m depth (see Vic et al., 2015; L'Hégaret et al., 2013).

On the profiles below the anticyclone (red circles) and below the cyclone (blue circles) on diagram Fig. 8, PGW has a density $\sigma_0 = 26\,\mathrm{kg\,m^{-3}}$ below the anticyclone, whereas it is denser under the cyclone with $\sigma_0 = 26.5\,\mathrm{kg\,m^{-3}}$. Thus, PGW below these eddies may have been captured at different times and locations, since the PGW outflow from the Persian Gulf presents varying characteristics with time.

The spiciness section (see Fig. 7, bottom) characterizes the thermohaline gradients across isopycnals, revealing the boundaries between the water masses. The most relevant feature of spiciness on the AS section lies around the mesoscale eddies: layers of cold and fresh water wrap around anticyclone A1 from 100 to 350 m depths, colocalized with maximal positive values of the Okubo–Weiss field. Maximal deformation created by A2 tore and wrapped IOCW around the eddy. An other layer of cold IOCW was recorded around C2, between 16.5 and 17° N.

In summary, in the Arabian Sea, the surface circulation is dominated by mesoscale eddies, primarily along the coast. Their strong vorticity in the upper layer separates ASHSW from water masses below. These eddies also have a deep vertical influence so that thus trap horizontally, displace vertically and mix the water masses below them. Under the anticyclone, the temperature of PGW is 2 °C colder under the cyclone. The difference in temperature can either result from a vertically heat flux between the eddies and these deeper water masses, or from the advection of a specific part only (e.g. the

OSD
12, 2743–2782, 2015

upper or lower part), of these water masses, under the eddies. They can also wrap IOCW and PGW around them, as layers. Submesoscale structures (filaments), with homogeneous water masses, are advected between the main eddies.

4.2 Sea of Oman

From 22 to 30 March the Phys-Indien experiment performed cross-sections in the Sea of Oman. A composite section (SO section) crossing this basin zonally, is presented and described here.

The MADT map above SO shows a positive anomaly (see Fig. 6), formed from a westward propagating signal, which entered the Sea of Oman in December 2010. The relative vorticity map reveals that the western part of the basin is occupied by smaller eddies. Thus, from west to east, SO crossed three alternating anticyclones and cyclones. The most energetic eddy, A1, laid in the eastern part of the Sea of Oman, with the highest velocities, up to 25 $cm\,s^{-1}$. The Okubo–Weiss quantity is negative in the center of A1, indicating a dominance of rotation, but positive in the western part, undergoing deformation.

As in the Arabian Sea, the maximal velocities of the eddies laid in the upper 150 m (see Fig. 9, top), but a secondary maximum was found west of 57.5° E; intense velocities near the surface corresponded to the exchange flow near the Strait. The geostrophic velocities, calculated from the SeaSoar density shows the same change in sign on the surface, but presents the higher velocities at the depth of the PGW.

The EPV field between 50 and 100 m depth is negative, as expected from the anticyclonic surface signature in the MADT, a positive maximum is found in the westernmost part of the section, characteristic of cyclonic eddies (see Fig. 9, middle). At depth, a positive peak in the EPV field is observed between 58 and 58.7° E, where Okubo–Weiss shows that deformation dominated over rotation. Furthermore, the spacing between the isopycnals, and the velocity signature indicates a anticyclonic motion, underlining the presence a of lens.

OSD
12, 2743–2782, 2015

The thermohaline section (Fig. 9, bottom) presents, as in the Arabian Sea, three water masses. The ASHSW is colder than in the Arabian Sea, between 22 and 25 °C and a homogeneous salinity of 36.6 psu. Its bottom depth varied between 75 and 150 m depth. Below, the IOCW is observed with the lowest salinity, between 36.1 and 36.3, and temperature varied 15 and 21 °C. The PGW was found at two locations with two strong differences.

A first patch of PGW is observed on the western part of the section, with strong thermohaline anomalies, temperature between 21 and 22 °C, and salinity beyond 36.8 psu, up to 38 psu, with depth varying between 150 and 320 m depth. This layer was fragmented into smaller patches with the strongest observed thermohaline characteristics presented on the diagram Fig. 10; at 57.25° E (brown circles profile), between 57.5 and 57.75° E (grey crosses profile) and between 57.9 and 58.2° E (green crosses profile). This water mass ceased at 58.8° E.

Oppositely, diluted PGW is observed on the eastern section, with temperature from 16 to 18 °C, salinity of 36.4 psu and between 275 and 350 m depth. These characteristics correspond to those measured below the cyclone in the Arabian Sea.

As in the Arabian Sea, the depth of equilibrium of the water masses depends of the mesoscale eddies, with a shallowing of the isopycnals between 58 and 59° E, where the relative vorticity map is positive, and a deepening east of 59.3° E, below the anticyclone (see Fig. 9, bottom). Nevertheless, between 57.5 and 57.75 and at 58° E, the isopycnals were stretched vertically between 250 and 350 m depth, at the position of the highest salinity of PGW, indicating an anticyclonic motion. Different submesoscale structures were observed here, filaments and lenses, described in the next section.

The spiciness also underlines the turbulent mixing, with injection of colder water and fresher water around the patches of PGW, resulting in a fragmented outflow water mass. Inside this patch, the layer can be vertically discompose, with the most saline water between 220 and 320 m depth, with $\sigma_0 = 26.2\,\mathrm{kg\,m^{-3}}$, and a second layer, between 150 and 230 m depth, with $\sigma_0 = 25.8\,\mathrm{kg\,m^{-3}}$. Around the eastern anticyclone,

OSD
12, 2743–2782, 2015

with the densest PGW at depth, an injection of saltier and warmer water inside this layer is observed.

The circulation in the Sea of Oman shows strong resemblance with that in the Arabian Sea. Mesoscale eddies, with lower intensity, dominate the flow at the surface and at depth. The water masses immersions depend of the pressure anomalies of the upper ocean layer. In the Sea of Oman the outflowing PGW is subject to strong mixing, and is fragmented, with detached rotating fragments at depth, and more isolated patches above. To the east of the gulf, beyond the strongest velocity front between surface eddies, the outflow is not clearly observed; the few Persian Gulf water patches have thermohaline values characteristic of mixing with the oceanic water, thus indicating a change of direction of the flow. This change occurred offshore of Ra's Al Hamra, as described in a previous section.

The spreading of the PGW during the Phys-Indien experiment is of interest, due to its variability in position, depth and characteristics. Hereafter the focus is put on its recording during the experiment.

5 PGW characteristics, pathway and submesoscale structures

On the θ/S diagrams of Figs. 8 and 10, an important feature of the PGW is the peaks in salinity at two different density ranges. A first one, lighter and fresher, with σ_0 between 25.8 and 26 $\mathrm{kg\,m^{-3}}$ is found on the profiles in the western Sea of Oman and below the anticyclones A1 and A3 with a salinity around 37 psu. This peak is also observed with diluted characteristics inside the core of the eddies in the western Sea of Oman and Arabian Sea and with salinity below 36.4 psu. A second peak, with higher salinity and denser, is found in the eastern Sea of Oman with a salinity of 37.9 psu, below the eddies with a salinity varying from 36.4 to 36.6 psu, and inside the lens off Ra's Al Hadd with a peak at 37.4 psu. These two peaks correspond to Persian Gulf Water from different seasons. The lighter outflow presents higher temperature and lower salinity (see Table 1). During the summer monsoon and at the beginning of the winter monsoon, the

OSD
12, 2743–2782, 2015

outflowing Persian Gulf Water is warmer, up to 23 °C in November; it is colder (about 21 °C) from February to May. Salinity also varies with a maximum between December and May and with a peak in April and May, around 38.5 psu. In summer and early winter PGW salinity decreases by about 1 psu, with a value around 37.3 in November. Thus the lightest waters outflow between July and August and in November, while the densest are observed in winter and spring.

Maps Fig. 11 indicate the maximal salinity in the PGW layer, and the associated temperature, potential density and spiciness; maps of Eulerian transport (Fig. 12) are computed to follow the pathways of the PGW outflows. The Eulerian transports can be related to the velocity sections and to the altimetric maps. Indeed, in the Sea of Oman, between 58.5 and 60° E, the volumic transport was anticyclonic, and also between 57 and 58.5° E. This corresponds to A1 and A3. In the Arabian Sea, the strong jet between C1 and A2 led to the 6.43 Sv transport eastward at 20.5° N, while an opposite westward jet between A2 and C2 at 18° N transported 2.77 Sv.

In the Sea of Oman, the front already seen in the SO section appeared with warm and salty PGW west of 59° E, and fresher waters with patches of higher spiciness east of 59° E. This front was created by the strong anticyclone A1, which stopped the zonal spreading of the PGW and advected it northward. The penetrating IOCW is also blocked from the east by the front, as observed on the recording of an ARGO float (number 2901370) in March 2011 (see Fig. 13). Differences between the altimetric map and the transport map can be due to the effect of bathymetry or of thermocline density gradients.

In the western Sea of Oman, newly outflowing PGW, cascaded down the southern continental slope, where the saltiest PGW was observed (see brown, red and yellow circle profiles Fig. 10, top). In late March, the anticyclonic circulation of the basin pushed the water westwards (see transport Fig. 12, top). This motion is observed on an ARGO float (number 2901387, see Fig. 13), looping cyclonically from March to May, then moving northwestward, towards the Strait. This recirculation, associated with the

OSD
12, 2743–2782, 2015

one induced by A1, forced the water to remain in the western part of the basin, thus leading to the presence of PGW from two different seasons in the same region.

These turbulent motions disrupted the outflowing PGW to stretch patches or lenses or filaments wrapping around the eddies, as in the western Sea of Oman. PGW was found at the periphery of A1 and A3 (see Fig. 10, blue diamond profile, top; cyan cross profile, bottom) with high salinity, diluting before penetrating the core of these eddies (see Fig. 10, bottom, red circle profile), with a difference of about 0.8 psu between the periphery and the core. The recent, winter, denser PGW, was mainly observed in the western eddy, whereas older or mixed PGW, lighter, was found in the eastern one.

In March 2011, the PGW mainly exited the Sea of Oman north, around the anticyclonic motion, but small patches below 36.8 psu were observed, confined to the coast, between Ra's Al Hamra and Ra's Al Hadd at 59° E–23.75° N and at 59.5° E–23.5° N (see Fig. 10, bottom, green diamonds profiles). The presence of both PGW types, well mixed, indicates that these fragments were formed during the spring monsoon, a few days before the experiment, probably due to a coastal pulse (see L'Hégaret et al., 2015).

In the Arabian Sea, the PGW motion around the eddies C1 and A2 was similar to that in the Sea of Oman but with stronger dilution, by more than 1 psu (see Fig. 8). In the A2 anticyclone, the PGW layer was warmer (see Fig. 11, top, left), with temperature above 19.5 °C,a priori due to heat transfer from the ASHSW layer in this intense eddy. South of 18° N, the PGW was strongly diluted and mixed with the IOCW.

An interesting feature of the water masses is observed around the strong mesoscale eddies, and lenses: injections of colder and fresher IOCW occur around them both in the Arabian Sea and in the Sea of Oman (see Fig. 8, cyan diamond profile). These structures present no front in density but a marked one in spiciness (see Fig. 7). Smith and Ferrari (2009) suggested that these filaments could here result from the stirring of PGW by the mesoscale eddies. The slope of these structures is compared with the f/N ratio, and with the strain over shear ratio induced by the eddies. The isospice slope varies from 0.3 to 0.4 %, f/N from 6×10^{-3} to 7×10^{-3}, and $\mathrm{d}U/\mathrm{d}x/\mathrm{d}U/\mathrm{d}z$ is very

Discussion Paper | Discussion Paper | Discussion Paper | Discussion Paper |

OSD

12, 2743–2782, 2015

Mesoscale eddies and submesoscale structures of Persian Gulf Water

P. L'Hégaret et al.

close to the isospice slope. This suggests that stirring can form these lateral injections. Furthermore, the presence of these colder and fresher injections below warmer and saltier PGW water favors double diffusion. This might be an explanation for the salty patch observed below the ASHSW layer on the southern profile (yellow diamonds in Fig. 8).

5.1 Submesoscale lens off Ra's Al Hadd

The lens section displayed on Fig. 6 corresponds to the measurements achieved between the 19 and the 20 March 2011. This section off Ra's Al Hadd extends between the southern cyclone C1 described earlier and the eastern part of anticyclone A3 at the mouth of the Sea Of Oman. The surface vorticity field indicates that the cyclone was more energetic than the anticyclone. This is also observed on the Okubo–Weiss field: the section is located in a region where deformation dominated rotation; indeed deformation reached there its maximal value observed in the Sea of Oman and Arabian Sea at this period. Note that the velocity induced by the mesoscale eddies was above $0.5\,\mathrm{m\,s^{-1}}$ in the southern part of the section.

The velocity section (Fig. 14, top) shows that the signature of the cyclone extends below 1000 m depth in the southern part of the section and below 400 m depth in the northern part. Between 22.1 and 22.4° N and 250 and 400 m depth, an anticyclonic motion is observed on the zonal velocity section with speed of about $20\,\mathrm{cm\,s^{-1}}$, but strongly dominated by the velocity of the surface eddy. The Okubo–Weiss field structure (Fig. 14, center) indicates that the first 400 m of the ocean were dominated by the strong deformation field between the two eddies and that a maximum of deformation is observed at the depth of the lens. The presence of this lens is also indicated on the EPV section by the anomaly.

The thermohaline section confirms the presence of a lens shaped structure between 250 and 350 m depth, with a diameter of 25 km, a temperature of 19 °C and salinity over 37.3 psu at its center. On a perpendicular cross section (not presented here), the lens has a diameter of 33 km, indicating that it is elliptical, this is confirmed by a third

OSD
12, 2743–2782, 2015

section (not shown). Above the lens, a fresh layer of IOCW is found with temperature between 16 and 19 °C and salinity below 36 psu up to 100 m depth. The surface layer is occupied by ASHSW, with temperature between 26 and 21.5 °C and a salinity of 36.6 psu. At the depth of the lens, and surrounding it, mixed PGW is observed with temperature between 14 and 16 °C and salinity peaking at 36.3 psu. The total salt and of heat content, inside the 36.6 psu (or 18 °C) contour, is 2.59×10^{12} kg and 6.54×10^{19} J, and the lens volumic transport (across the section) is above 0.4 Sv. The density section on Fig. 14 (bottom, left) indicates the presence of this anticyclonic lens, with an increased spacing of the isopycnals between 250 and 350 m depth. The spiciness presents injections of neighbouring water beneath the lens, which are composed of upper IOCW.

A vertical profile (green cross profile on Fig. 8) and sections (see Fig. 14), indicate that this submesoscale lens has a density $\sigma_0 = 26.6\,\mathrm{kg\,m^{-3}}$, and a salinity above 37.3 psu; this salinity was observed only in the Sea of Oman at this period; therefore it is likely that this sea was the formation site of this lens. In L'Hégaret et al. (2015), several mechanisms leading to the formation of eddies containing PGW were cited. Hereafter, two most probable mechanisms are assessed. In winter, the formation of coastal lee eddies is observed, downstream of Ra's Al Hamra; these eddies retain high salinity in their core before eroding during three months. This mechanism was observed in the high resolution, HYCOM simulation, and lee eddies were the only structure carrying salinity above 37 psu in the Arabian Sea and possessing a strong altimetric signature. No such signature was seen in the MADT anomaly maps of January to March 2011.

The other possible mechanism for the formation of this lens in the Sea of Oman would be the ejection of PGW fragments by mesoscale eddies. This can occur at Ra's Al Hamra or south of Ra's Al Hadd. In the Sea of Oman, the maximal deformation affecting the PGW outflow occurred near Ra's Al Hamra. This mechanism implies that the PGW lens would have drifted about 600 km, around anticyclone A2. The anticyclone velocity was at least $40\,\mathrm{cm\,s^{-1}}$ at the depth of the outflow. It would have taken 15 days for the lens to travel this distance; this corresponds to a formation in early March. An-

OSD
12, 2743–2782, 2015

other possible formation site is south of Ra's Al Hadd. Cyclone C1 would have ejected the lens and advected it. With a velocity of about $60\,\mathrm{cm\,s^{-1}}$, it would have taken 10 days between the time of ejection and that of measurements. Nevertheless, the high salinity of the lens is more indicative of formation from the PGW outflow near Ra's Al Hamra.

During the Phys-Indien 2011 experiment, two surdrift floats and three ARGO floats were seeded in the submesoscale lens. The surdrift floats allowed a hourly tracking of the lens, and the ARGO floats recorded temperature and salinity with a surfacing every 5 days. All these floats followed a northwestward trajectory for the first 4 days of measurements. After this period, the three ARGO floats were ejected, as revealed by their recorded salinity; so were the surdrifts which then followed anticylone A3, north of Ra's Al Hadd. One surdrift buoy lost its drogue and performed inertial loops. This inability to track the lens for long underlines the strong deformation that it was subjected to. Ruddick (1987) studied the deformation of a vortex lens by shear and strain. As the strain increases, the lens become more elliptical and unsteady, before either breaking up or readjusting. The surdrift loops reducing in size and velocity, and then following the mesoscale anticyclonic flow are coherent with a break up of the submesoscale PGW lens.

5.2 Recurrence of PGW lenses in the region

Numerous vertical sections from the ARGO floats (WHOI numbers 1901187, 1901202 and 6900902) revealed the presence of PGW at the mouth of the Sea of Oman. Until the early summer monsoon, localized patches of water with salinity above 37.2 psu, temperature around 20 °C and $\sigma_0 \approx 26.5\,\mathrm{kg\,m^{-3}}$ are observed, with a spacing of the isopycnals above and below. These lenses are found either off Ra's Al Hadd or off the Sea of Oman. In June 2011, anticyclone A3 was advected northward as the summer monsoon began, thus reducing the deformation field off Ra's Al Hamra. Since a strong shear and strain is necessary to break the PGW outflow and to form lens and filaments, it is logical to observe fewer submesoscale PGW structures during the summer monsoon.

OSD
12, 2743–2782, 2015

6 Conclusions

The Phys-Indien experiment took place in March 2011, during the spring inter monsoon. The surface signature was dominated by mesoscale eddies along the western coast of the Arabian Sea. A strong mesoscale anticyclone was observed in the eastern part of the Sea of Oman, characteristic of the spring inter monsoon; it was associated with a coastal ejection of PGW off Ra's Al Hamra.

The energetic mesoscale eddies have a strong vertical influence and deepen or shallow the water masses below them (ASHSW, IOCW and PGW). Inside these eddies cores, these water masses keep the thermohaline characteristics at the time of their trapping; PGW filaments wrapping around these eddies are subject to strong dilution. Besides, injections, primarily of cold and fresh IOCW, occur around the eddies, thus inducing mixing, and dilution of the highly saline waters.

In the western Sea of Oman, the PGW outflow appears fragmented, forming small eddies, filaments and a few isolated patches. Two layers of PGW, with different densities, from the winter monsoon and earlier mixed PGW, were observed at the same location, due to the anticyclonic recirculation in the western basin. The PGW outflow was not observed in the measurements along the coast between Ra's Al Hamra and Ra's al Hadd, with the exception of a few small coastal patches; PGW was advected north, around anticyclones A1 and A3, slowly diluted along its pathway, with a salinity below 37 psu.

A submesoscale lens recorded off Ra's Al Hadd possessed strong salinity (over 37 psu) and temperature, characteristic of the winter monsoon. Different hypotheses are proposed for its formation; this lens could have resulted either from a lee eddy eroding since the late winter, or from the fragmentation of the PGW outflow, at Ra's Al Hamra or south of Ra's Al Hadd, 15 or 10 days before the recording. This submesoscale lens was then observed between two strong mesoscale eddies during the Phys-Indien experiment, and having an elliptical structure. These mesoscale eddies deformed the lens, making it unsteady, and most likely, it rapidly disappeared afterwards.

OSD
12, 2743–2782, 2015

This mesoscale eddy shear/strain supports the formation of lenses from the coastal PGW outflow during the spring inter monsoon; this is supported by the repeated observations of such submesoscale patches of PGW, both with the SeaSoar and with the ARGO floats. But simultaneously the deformation field, induced by the mesoscale gyres, makes these lenses subject to break up, particularly out of the Sea Of Oman.

Thus, spring presents the most favourable conditions for PGW lens detection, with their ejection from the coastal outflow, and their advection around mesoscale eddies. During the summer monsoon, the PGW outflow is then expelled by the Ra's Al Hadd jet, an intense mesoscale surface dipole, which may disrupt the PGW fragments shortly after their formation. In March 2014, a second Phys-Indien took place around the Arabian Peninsula with a different mesoscale circulation, the study and comparision with spring 2011 situation of the PGW outflow forms will be the subject of a further study.

References

Al Saafani, M., Shenoi, S., Shankar, D., Aparna, M., Kurian, J., Durand, F., and Vinayachandran, P.: Westward movement of eddies into the Gulf of Aden from the Arabian Sea, J. Geophys. Res.-Oceans, 112, C11004, doi:10.1029/2006JC004020, 2007. 2745

Barth, J. A., O'Malley, R. T., Fleischbein, J., Smith, R. L., and Huyer, A.: SeaSoar and CTD observations during coastal jet separation cruise W9408A, August to September 1994, Tech. rep., College of Oceanic and Atmospheric Sciences, Corvallis, OR, USA, 1996. 2748

Bower, A. S. and Furey, H. H.: Mesoscale eddies in the Gulf of Aden and their impact on the spreading of Red Sea Outflow Water, Prog. Oceanogr., 96, 14–39, 2012. 2745

Carton, X., L'Hegaret, P., and Baraille, R.: Mesoscale variability of water masses in the Arabian Sea as revealed by ARGO floats, Ocean Sci., 8, 227–248, doi:10.5194/os-8-227-2012, 2012. 2745, 2746, 2753

Chelton, D. B., Deszoeke, R. A., Schlax, M. G., El Naggar, K., and Siwertz, N.: Geographical variability of the first baroclinic Rossby radius of deformation, J. Phys. Oceanogr., 28, 433–460, 1998. 2745

Ducet, N., Le Traon, P.-Y., and Reverdin, G.: Global high-resolution mapping of ocean circulation from TOPEX/Poseidon and ERS-1 and-2, J. Geophys. Res.-Oceans, 105, 19477–19498, 2000. 2747

Fischer, A. S., Weller, R. A., Rudnick, D. L., Eriksen, C. C., Lee, C. M., Brink, K. H., Fox, C. A., and Leben, R. R.: Mesoscale eddies, coastal upwelling, and the upper-ocean heat budget in the Arabian Sea, Deep-Sea Res. Pt. II, 49, 2231–2264, 2002. 2745

Fu, L.-L., and Cazenave, A.: Satellite Altimetry and Earth Sciences: A Handbook of Techniques and Applications, vol. 69, Academic Press, San Diega, CA, USA, 2000. 2747

Hoskins, B.: The role of potential vorticity in symmetric stability and instability, Q. J. Roy. Meteor. Soc., 100, 480–482, 1974. 2751

IOC, SCOR and IAPSO: The international thermodynamic equation of seawater – 2010: calculation and use of thermodynamic properties, Intergovernmental Oceanographic Commission, Manuals and Guides No. 56, UNESCO (English), 196 pp., 2010. 2750

Kumar, S. P. and Prasad, T.: Formation and spreading of Arabian Sea high-salinity water mass, J. Geophys. Res.-Oceans, 104, 1455–1464, 1999. 2746

L'Hégaret, P., Lacour, L., Carton, X., Roullet, G., Baraille, R., and Corréard, S.: A seasonal dipolar eddy near Ras Al Hamra (Sea of Oman), Ocean Dynam., 63, 633–659, 2013. 2746, 2752, 2755

L'Hégaret, P., Duarte, R., Carton, X., Vic, C., Ciani, D., Baraille, R., and Corréard, S.: Mesoscale variability in the Arabian Sea from HYCOM model results and observations: impact on the Persian Gulf Water path, Ocean Sci., 11, 667–693, doi:10.5194/os-11-667-2015, 2015. 2745, 2746, 2751, 2752, 2760, 2762

Lueck, R. G. and Picklo, J. J.: Thermal inertia of conductivity cells: observations with a Sea-Bird cell, J. Atmos. Ocean. Tech., 7, 756–768, 1990. 2748

Meshal, A. and Hassan, H.: Evaporation from the coastal water of the central part of the Gulf, Arab Gulf Journal of Scientific Research, 4, 649–655, 1986. 2745

Ollitrault, M. and Rannou, J.-P.: ANDRO: an argo-based deep displacement dataset, J. Atmos. Ocean. Tech., 30, 759–788, 2013. 2747

Pous, S., Carton, X., and Lazure, P.: Hydrology and circulation in the Strait of Hormuz and the Gulf of Oman results from the GOGP99 experiment: 2. Gulf of Oman, J. Geophys. Res.-Oceans, 109, doi:10.1029/2003JC002146, 2004. 2746

OSD
12, 2743–2782, 2015

Premchand, K., Sastry, J., and Murty, C.: Watermass structure in the western Indian Ocean, part II, The spreading and transformation of the Persian Gulf Water, Mausam, 37, 179, doi:10.1029/2000JC000480, 1986. 2746

Privett, D.: Monthly charts of evaporation from the N. Indian Ocean (including the Red Sea and the Persian Gulf), Q. J. Roy. Meteor. Soc., 85, 424–428, 1959. 2745

Reynolds, R. M.: Physical oceanography of the Gulf, Strait of Hormuz, and the Gulf of Oman results from the Mt Mitchell expedition, Mar. Pollut. Bull., 27, 35–59, 1993. 2745

Rio, M., Guinehut, S., and Larnicol, G.: New CNES-CLS09 global mean dynamic topography computed from the combination of GRACE data, altimetry, and in situ measurements, J. Geophys. Res.-Oceans, 116, C07018, doi:10.1029/2010JC006505, 2011. 2747

Ruddick, B. R.: Anticyclonic Lenses in Large-Scale Strain and Shear, J. Phys. Oceanogr., 17, 741–749, doi:10.1175/1520-0485(1987)017<0741:ALILSS>2.0.CO;2, 1987. 2763

Smith, K. S. and Ferrari, R.: The production and dissipation of compensated thermohaline variance by mesoscale stirring, J. Phys. Oceanogr., 39, 2477–2501, 2009. 2760

Teague, W. J., Carron, M. J., and Hogan, P. J.: A Comparison between the Generalized Digital Environmental Model and Levitus Climatologies, Tech. rep., Naval Oceanographic and Atmospheric Research Laboratory at the Stennis Space Center, MS, USA, DTIC Document, 1990. 2747

Thoppil, P. G. and Hogan, P. J.: On the mechanisms of episodic salinity outflow events in the Strait of Hormuz, J. Phys. Oceanogr., 39, 1340–1360, 2009. 2754

Vic, C., Roullet, G., Carton, X., and Capet, X.: Mesoscale dynamics in the Arabian Sea and a focus on the Great Whirl life cycle: a numerical investigation using ROMS, J. Geophys. Res.-Oceans, 119, 6422–6443, 2014. 2751

Vic, C., Roullet, G., Capet, X., Carton, X., Molemaker, M., and Gula, J.: Eddy-topography interactions and the fate of the Persian Gulf Outflow, J. Geophys. Res.-Oceans, 120, doi:10.1002/2015JC011033, 2015. 2755

Table 1. Maximal PGW density, and associated salinity and temperature, before cascading in the Sea of Oman for each month extracted from the GDEM climatology.

Month	Jan	Feb	Mar	Apr	May	Jun
Density ($kg\,m^{-3}$)	26.62	26.61	26.82	26.95	26.92	26.32
Salinity (psu)	38.46	38.26	38.29	38.48	38.50	37.89
Temperature ($^{\circ}C$)	22.79	22.31	21.66	21.70	21.87	22.33
Month	**Jul**	**Aug**	**Sep**	**Oct**	**Nov**	**Dec**
Density ($kg\,m^{-3}$)	25.91	26.01	26.25	26.01	25.74	26.34
Salinity (psu)	37.53	37.63	37.83	37.66	37.32	38.29
Temperature ($^{\circ}C$)	22.80	22.74	22.42	22.78	22.84	23.32

OSD
12, 2743–2782, 2015

Mesoscale eddies and submesoscale structures of Persian Gulf Water

P. L'Hégaret et al.

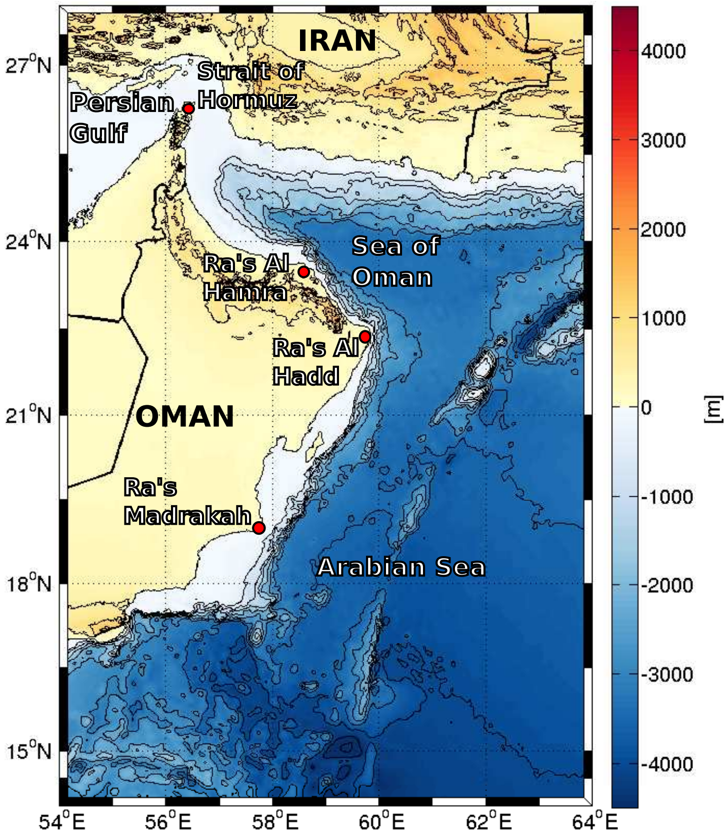

Figure 1. Topographic map of the Arabian Sea and Sea of Oman with the locations of interest.

OSD
12, 2743–2782, 2015

Mesoscale eddies and submesoscale structures of Persian Gulf Water

P. L'Hégaret et al.

Title Page
Abstract
Introduction
Conclusions
References
Tables
Figures
Back
Close
Full Screen / Esc
Printer-friendly Version
Interactive Discussion

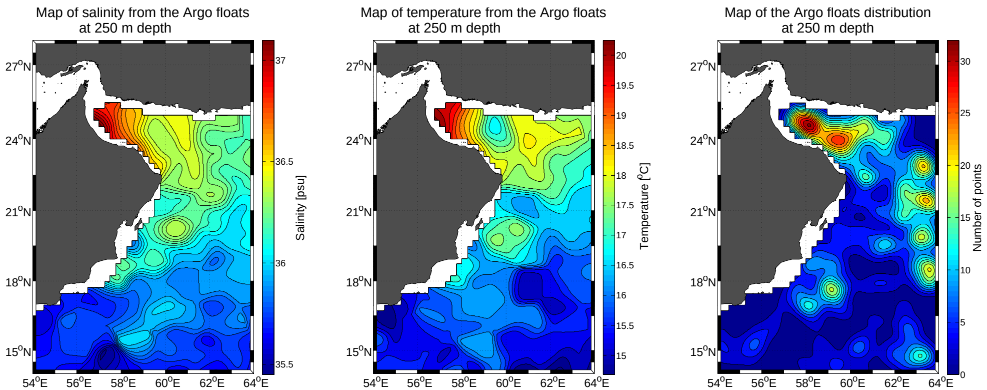

Figure 2. Maps of the salinity (left) and temperature (center) from GDEM modified by ARGO floats at 250 m depth for a climatological month of March; associated number of floats is indicated on the right-hand panel.

OSD
12, 2743–2782, 2015

Mesoscale eddies and submesoscale structures of Persian Gulf Water

P. L'Hégaret et al.

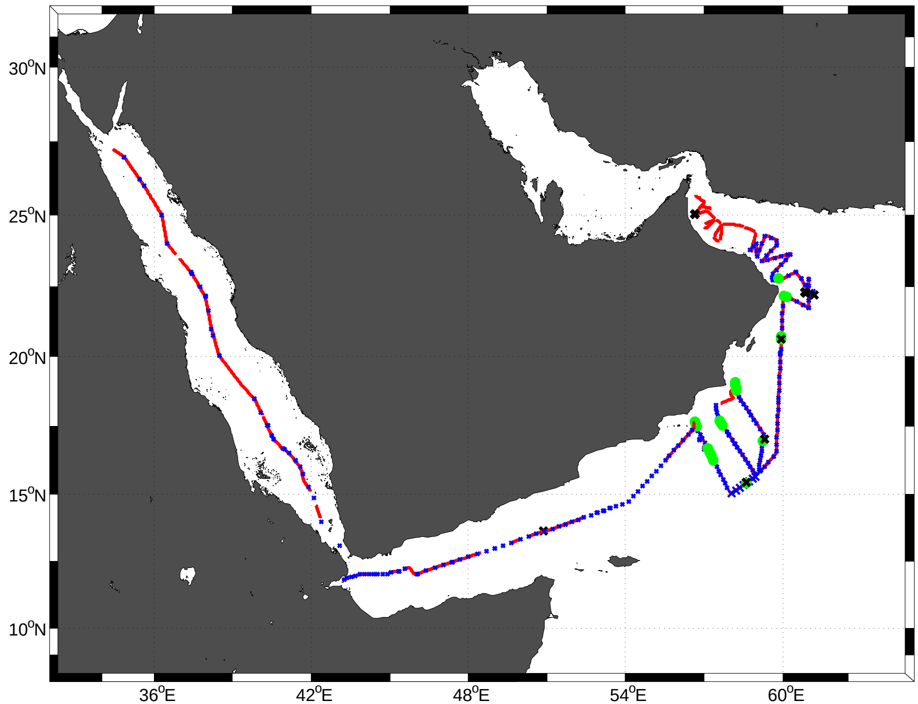

Figure 3. Location of the Phys-Indien 2011 measurements. The red line follows the VM-ADCP and SeaSoar lines (with the exception of the Red Sea and Gulf of Aden where only the VM-ADCP was activated). The blue crosses and green circles represent the positions of XBT-XCTD casts and of CTDL-ADCP stations respectively. The black crosses represent the launch positions of floats (Surdrift and PROVOR).

OSD
12, 2743–2782, 2015

Mesoscale eddies and submesoscale structures of Persian Gulf Water

P. L'Hégaret et al.

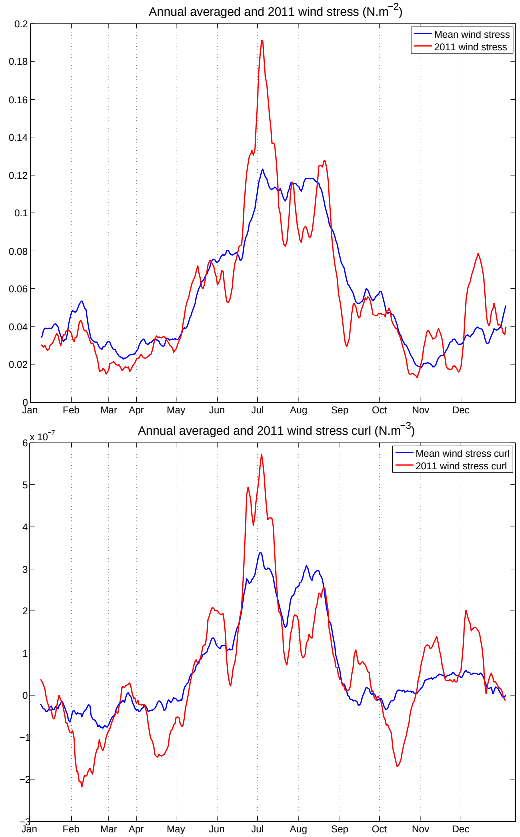

Figure 4. Daily wind stress (upper panel) and wind stress curl (lower panel) in blue and their 15 day means in red, over a 2° square region off Ra’s Al Hadd.

OSD
12, 2743–2782, 2015

Mesoscale eddies and submesoscale structures of Persian Gulf Water

P. L’Hégaret et al.

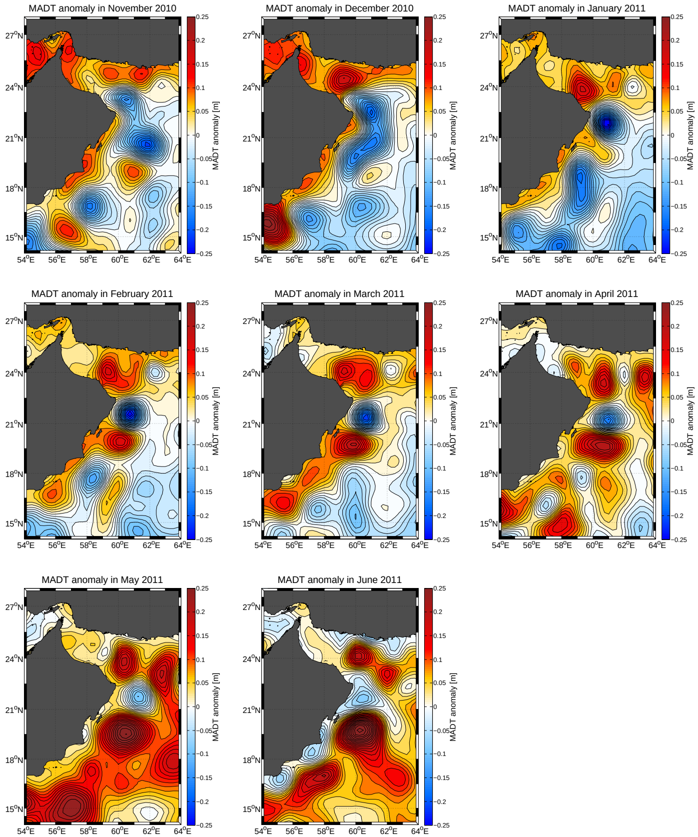

Figure 5. Maps of the MADT (altimetric) anomaly averaged over a month, from November 2010 to June 2011.

OSD
12, 2743–2782, 2015

Mesoscale eddies and submesoscale structures of Persian Gulf Water

P. L'Hégaret et al.

Title Page
Abstract | Introduction
Conclusions | References
Tables | Figures
◀| |▶
◀ ▶
Back | Close
Full Screen / Esc
Printer-friendly Version
Interactive Discussion

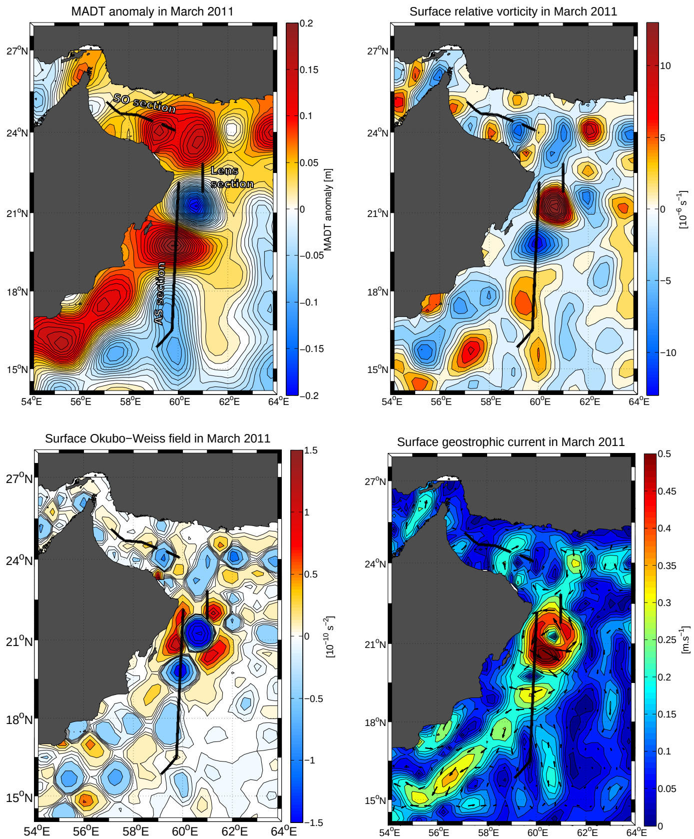

Figure 6. Maps of the surface fields averaged from 16 to 30 March 2011, during the measurements south of Ra's Al Hadd (AS section), in the lens off Ra's Al Hadd (lens section), and across the Sea of Oman (SO section). Fields are: ADT anomaly (top, left); relative vorticity (top, right); Okubo–Weiss criterion (bottom, left); geostrophic velocity (bottom, right).

OSD
12, 2743–2782, 2015

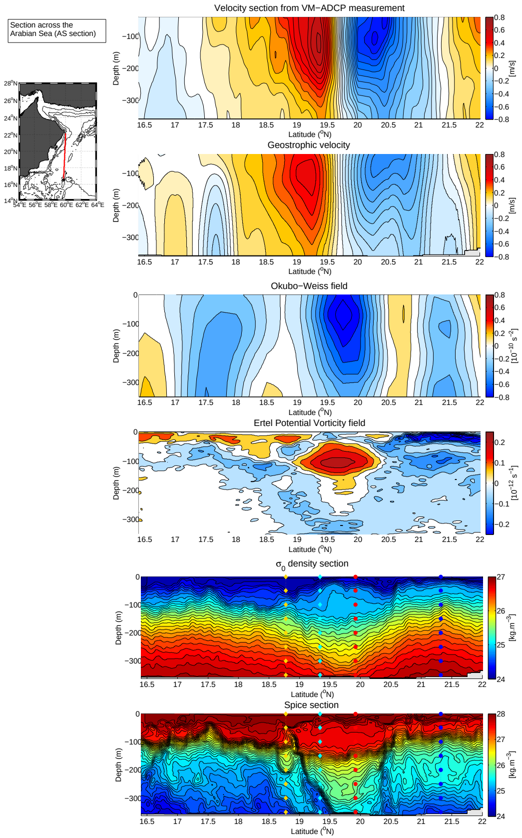

Figure 7. AS sections of the eddies, south of Ra's Al Hadd from surface down to 350 m depth. Measurements are: VM-ADCP and geostrophic velocities (from SeaSoar density), positive towards the west; Okubo–Weiss paramater calculated from the ARGO-GDEM density and velocity fields and Ertel Potential Vorticity from VM-ADCP and SeaSoar fields; σ_0 potential density and spiciness.

OSD
12, 2743–2782, 2015

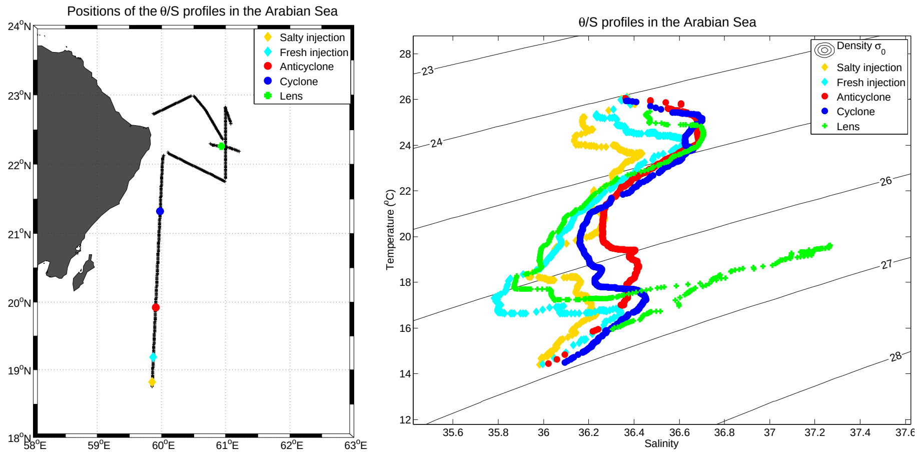

Figure 8. Potential temperature over salinity profiles (right) in the western Arabian Sea at various locations of interest (left). From north to south: yellow diamond: salty injection around the anticyclone A2; cyan diamond: fresh injection around the anticyclone A2; red circle: inside the anticyclone A2; blue circle: inside the cyclone C1; green cross, at the periphery of the anticyclone; red circle: inside the lens off Ra's Al Hadd.

OSD
12, 2743–2782, 2015

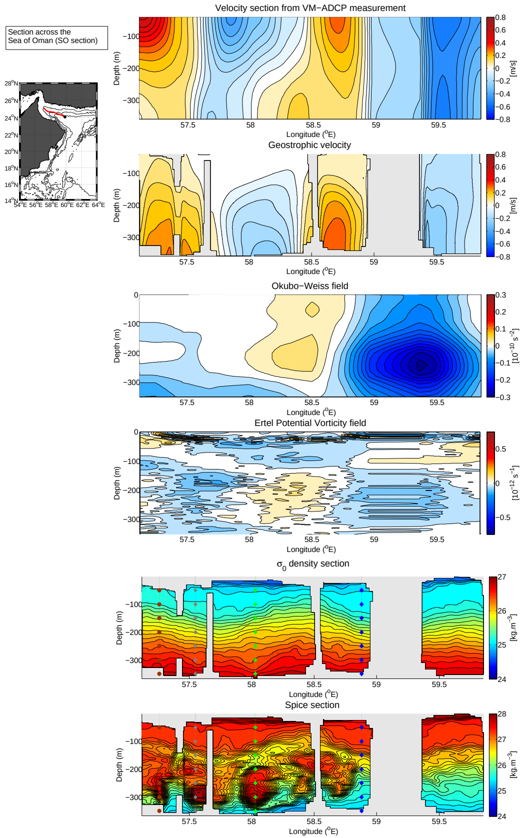

Figure 9. SO sections of the eddies, south of Ra's Al Hadd from surface down to 350 m depth. Measurements are: VM-ADCP and geostrophic velocities (from SeaSoar density), positive towards the north; Okubo–Weiss paramater calculated from the ARGO-GDEM density and velocity fields and Ertel Potential Vorticity from VM-ADCP and SeaSoar fields; σ_0 potential density and spiciness.

OSD
12, 2743–2782, 2015

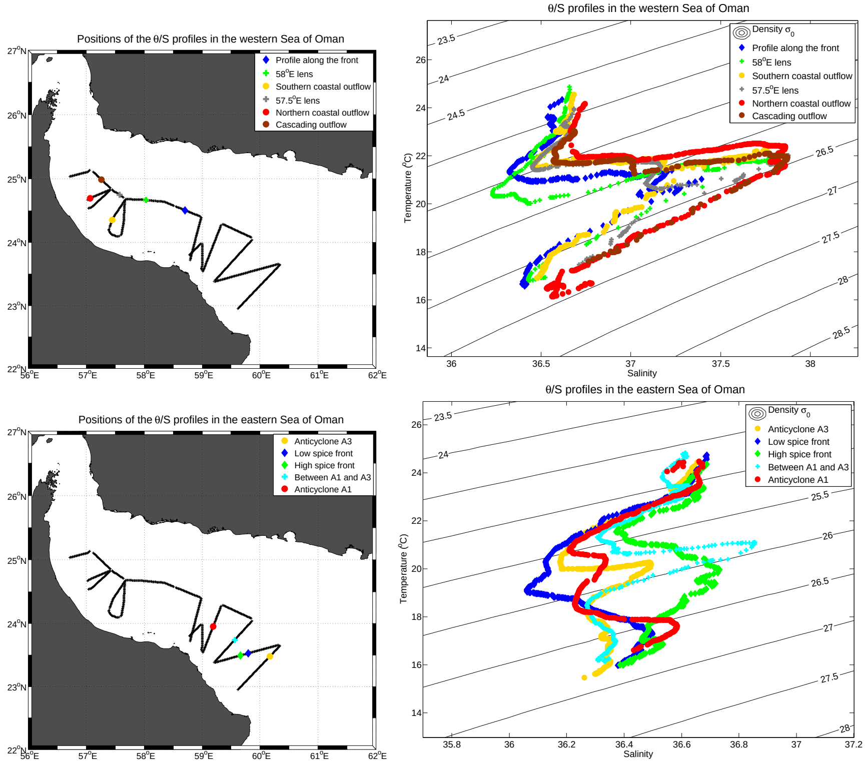

Figure 10. Potential temperature over salinity profiles (right panels) and their locations of interest (left panels); in the western Sea of Oman (upper panels) and eastern Sea of Oman (lower panels). Upper left panel: blue diamond: profile out of the salty outflow; green cross: 58° E lens; yellow circle: southern profile in the PGW outflow along the coastal slope; grey/black cross: 57.5° E lens; red circle: northern profile in the PGW outflow along the coastal slope; brown circle: cascading PGW outflow. Lower left panel: yellow circle: profile inside the anticyclone A3; blue diamond: low spice profile; green diamond: high spice profile; cyan cross: at the periphery of the anticyclones A1 and A3; red circle: profile inside the anticyclone A1.

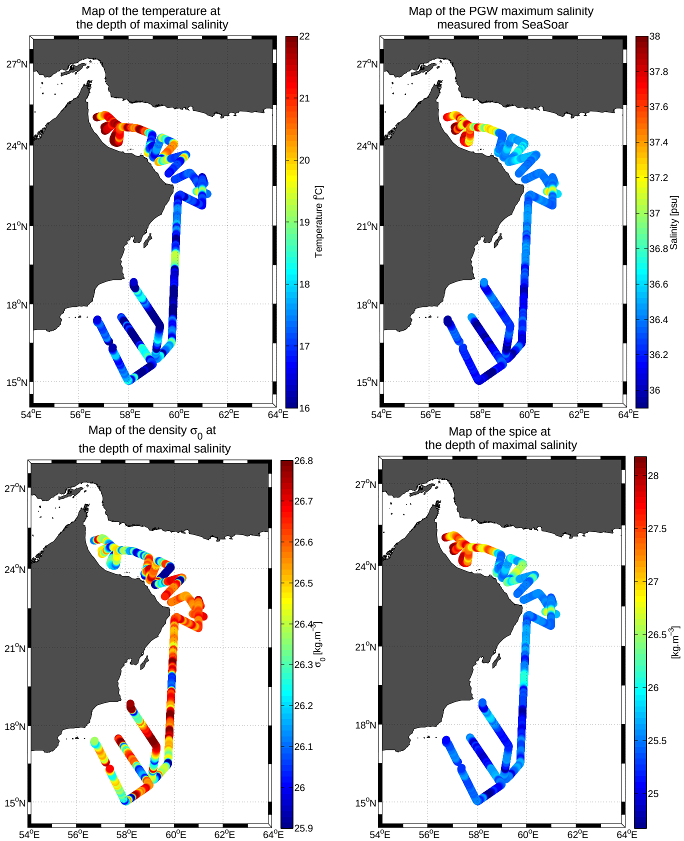

Figure 11. Scatter maps from the SeaSoar measurements displaying the maximal thermohaline characteristics of the Persian Gulf Water (for σ_0 between 26 and 26.7). The variables are: temperature (top, left); salinity (top, right); σ_0 at the maximal salinity depth (bottom, left); and spiciness at the same depth (bottom, right).

OSD
12, 2743–2782, 2015

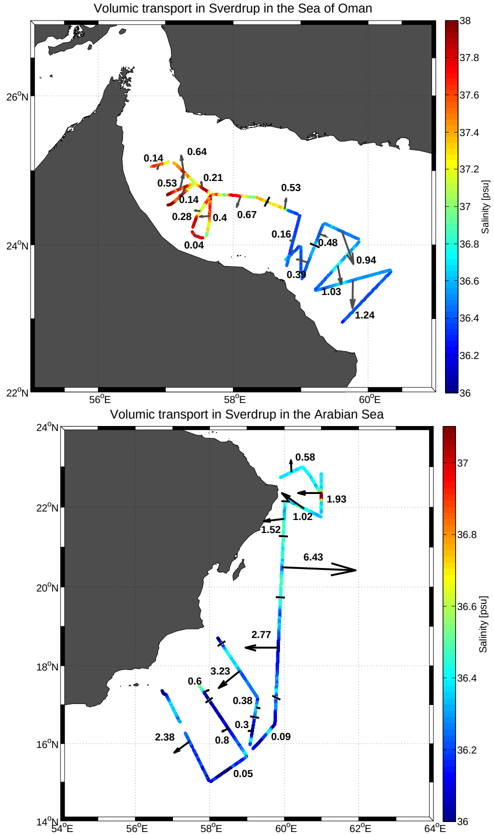

Figure 12. Eulerian volumic transport across the SeaSoar measurements in the Sea of Oman (top) and in the Arabian Sea (bottom). Arrows indicates the direction, the values are in Sverdrup and in color is indicated the maximum of salt in the PGW layer.

OSD
12, 2743–2782, 2015

Mesoscale eddies and submesoscale structures of Persian Gulf Water

P. L'Hégaret et al.

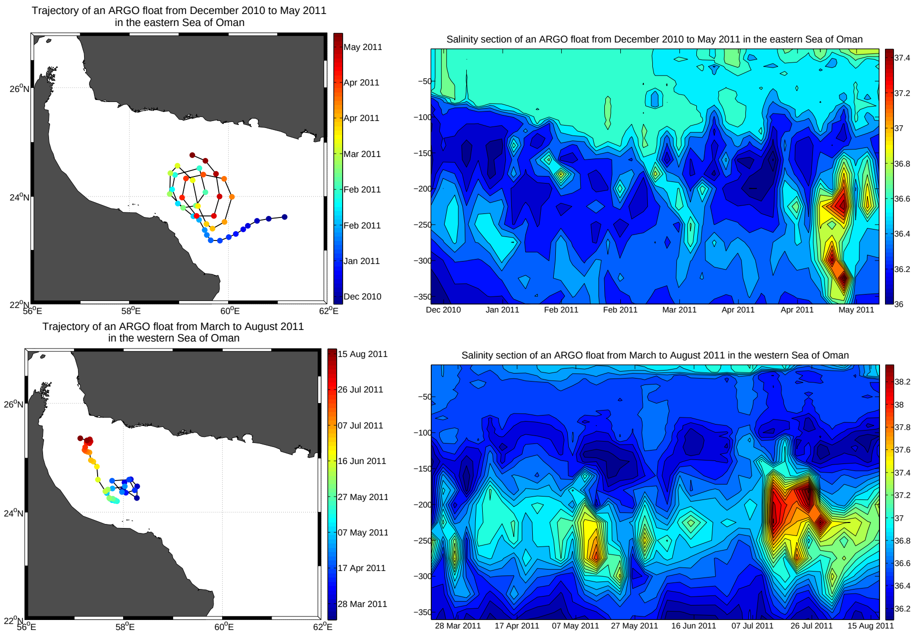

Figure 13. ARGO floats 2901370 (upper panels) and 2901387 (lower panels), trajectories (left) and salinity section (right) in the eastern and western Sea of Oman. Float 2901370 (up) enters the Sea of Oman with anticyclonic loops, is stopped by the front in March 2011 and then looped cyclonically until late May 2011, between A1 and A3. Float 2901387 looped cyclonically from March to May 2011 before moving northwest. Patches of salty PGW are observed, with the strongest in July when the float is found near the position of cascading PGW.

OSD
12, 2743–2782, 2015

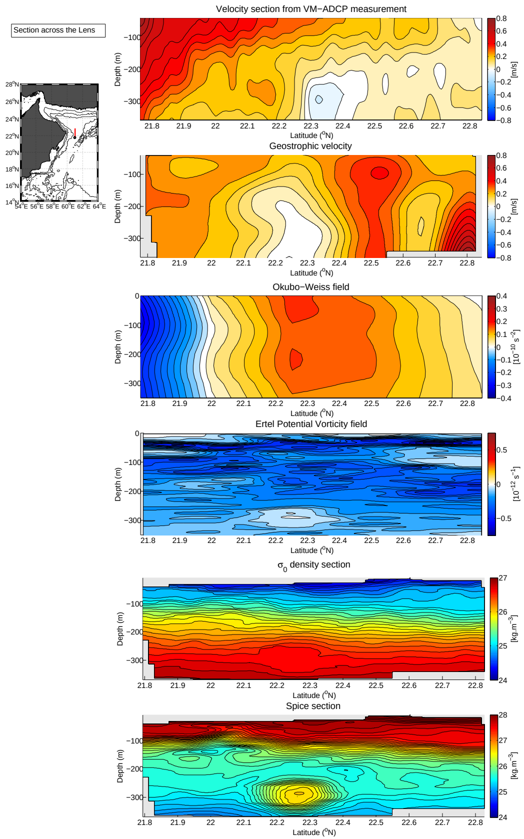

Figure 14. Sections across the lens off Ra's Al Hadd from surface down to 350 m depth. Measurements are: VM-ADCP and geostrophic velocities (from SeaSoar density), positive towards the west; Okubo–Weiss paramater calculated from the ARGO-GDEM density and velocity fields and Ertel Potential Vorticity from VM-ADCP and SeaSoar fields; σ_0 potential density and spiciness.

OSD

12, 2743–2782, 2015

Title Page
Abstract | Introduction
Conclusions | References
Tables | Figures
◀| |▶
◀ ▶
Back | Close
Full Screen / Esc
Printer-friendly Version
Interactive Discussion